Front. Earth Sci. 2015, 9(3): 394–411
DOI 10.1007/s11707-014-0437-8

RESEARCH ARTICLE

Determination of water flushing characteristics and their influencing factors on the Dahuofang Reservoir in China using an improved ECOMSED model

Ming ZHANG, Yongming SHEN (✉)

State Key Laboratory of Coastal and Offshore Engineering, Dalian University of Technology, Dalian 116023, China

Abstract A three-dimensional hydrodynamic model with the capability to deal with changing land water boundaries was developed based on ECOMSED in this study. The model was configured to numerically study the water flushing characteristics of Dahuofang Reservoir in China through the determination of spatially distributed residence times. The model successfully reproduced the intra-annual water level variations, as well as the temporal evolution and spatial distribution of water temperature. Through a series of numerical experiments, it can be concluded that (1) the water flushing of the reservoir is both temporally and spatially variable; and (2) inflows and withdrawals are the decisive factors influencing the water flushing characteristics. Heat fluxes are the controlling factors of the water flushing of a strong stratified reservoir. Wind has the weakest effect, but it still should be considered in determination of reservoir water flushing characteristics.

Keywords numerical modeling, residence time, flushing, influence factor, Dahuofang Reservoir

1 Introduction

Reservoirs are typically built to store water for various purposes, including water supply, irrigation, flood control, power generation, recreation, etc. However, reservoir development can result in a number of negative environmental and socio-economic impacts.

Numerous environmental and socio-economic consequences result from reservoir development (Dionne and Therien, 1997) with water pollution being one of the greatest concerns by both the government and the public in recent years. The water quality of an aquatic system depends, to a large extent, on the physical processes of transport and mixing that occur within it. The processes not only determine the spatial location of dissolved and suspended substances at any given instant, but also dictate the environmental conditions that control the occurrence of biogeochemical processes (Rueda et al., 2006; Zhang et al., 2010). A first-order description of the processes is most often referred to as the flushing or residence time (Bolin and Rodhe, 1973; Zimmerman, 1976; Takeoka, 1984; Monsen et al., 2002; Rueda et al., 2006; Cavalcante et al., 2012). This is a related concept to water exchange for representing the time scale of water renewal within an aquatic system (Delhez and Deleersnijder, 2012). Thus, determination of the residence time is important because the knowledge of water renewal time can significantly aid the assessment of the environmental state of water bodies and their sustainable management (Dabrowski et al., 2012).

Residence time is conceived as the time required for a dissolved or suspended material discharged into a water body to be transported out of defined boundaries. Increasing studies have been conducted in recent years to investigate residence time in reservoirs, estuaries, and seas, in areas such as, Canning Reservoir in Western Australia (Hocking and Patterson, 1994), Sau Reservoir in North-Eastern Spain (Rueda et al., 2006), Lough Corrib in the west of Ireland (Dabrowski and Berry, 2009), Hudson River estuary (Warner et al., 2010) and New York Bight in the U.S. (Zhang et al., 2010), Dahuofang Reservoir in China (Shen et al., 2011), Scheldt Estuary in Belgium and The Netherlands (de Brauwere et al., 2011), Yuan-Yang Lake in northeastern Taiwan (Liu et al., 2012), Palm Jumeirah Lagoon in Dubai, United Arab Emirates (Cavalcante et al., 2012), Gulf of Kachchh, northwestern Arabian Sea (Patgaonkar et al., 2012), Irish Sea in the U.K.

Received June 29, 2013; accepted December 24, 2013

E-mail: ymshen@dlut.edu.cn

(Dabrowski et al., 2012), Shihmen Reservoir in northern Taiwan (Liu and Chen, 2013), St. Louis Bay Estuary, Mississippi (Camacho and Martin, 2013) and Liverpool Bay in the U.K. (Phelps et al., 2013). Over time, the hydrodynamic model used in the studies gradually shifted from quasi-two- or two- to three-dimensional.

Since 2010, Dahuofang Reservoir, one of the nine key water supply sources of China, has supplied water to seven major cities of Liaoning Province. As a result, water features of the reservoir have become increasingly prominent and stand in an important strategic position in the socio-economic construction of the district (Shen et al., 2011). It is essential that the flow patterns and water flushing characteristics of the reservoir be well understood to better protect and utilize its water resources. Hitherto, only Shen et al. (2011) have conducted the efforts necessary to estimate the water renewal time of Dahuofang Reservoir. They studied the residence time by dividing the reservoir into seven segments and investigated how flows can influence the average residence time of each segment. It is believed that the water flushing properties of Dahuofang Reservoir are not well understood.

The objectives of this study are (1) to determine the water flushing properties of Dahuofang Reservoir through the estimation of spatially distributed residence times, and (2) to investigate how flows (including river inflows and withdrawals), wind, and heat fluxes influence them. In reservoir operation, water level must be maintained at a low level to retain a capacity to prevent flood in the flood season and at a high level to store water in the non-flood season. It is essential for a numerical model to have the capability to simulate the sharp water level fluctuation. Thus, a three-dimensional hydrodynamic model with the capability to deal with changing land water boundaries was developed for Dahuofang Reservoir. In particular, the hydrodynamic features obtained from simulation based on the developed model were compared with available field observations. The water flushing characteristics of the reservoir were then numerically examined through instantaneously releasing passive dissolved conservative tracers.

The layout of this paper is as follows. Section 2 describes the study area and the methodology. Section 3 provides the model setup and validation, followed by the presentation and discussion of the results from the residence time examinations in Section 4. Final conclusions are drawn in Section 5.

2 Materials and methods

2.1 Study area

Dahuofang Reservoir was completed in 1958 with an initial design capacity of 21.87×10^8 m^3 and a drainage area of 5,437 km^2, which make it the largest reservoir in Liaoning, China. It is located in the northeastern region of China between 41°31′N–42°15′N and 120°20′E–125°15′E and is a river-valley type reservoir (Fig. 1). The length of the reservoir is approximately 35 km with a maximum width of approximately 4 km and a minimum of 0.3 km. The reservoir has a maximum surface area (at the maximum flood level of 138.8 m) of 114 km^2 and a mean depth of 12 m with maximum depth of 37 m near the dam. The detailed features of the reservoir are presented in Table 1. The functions of the reservoir include flood control, irrigation, municipal and industrial water supply, fishery and hydropower generation, etc. To satisfy the increasing water resources demand, a water transfer project that transfers water from Fengming Reservoir to Dahuofang Reservoir was started in 2003. After the water transfer project was completed in 2008, a volume of 18.2×10^8 m^3 water could be imported into the reservoir annually. Since then, seven major cities (Fushun, Shenyang, Liaoyang, Anshan, Yingkou, Panjin, and Dalian) of Liaoning Province with a population over 20 million could benefit from the project.

Table 1 Characteristics of Dahuofang Reservoir

Parameter	Value
Drainage area/km^2	5,437
Maximum surface area/km^2	114
Total reservoir capacity/m^3	21.87×10^8
Flood control capacity/m^3	11.82×10^8
Beneficial reservoir capacity/m^3	12.76×10^8
Dead reservoir capacity/m^3	1.34×10^8
Maximum flood level/m	138.8
Normal water level/m	131.5
Flood control level/m	126.4
Dead water level/m	108
Maximum depth/m	37
Mean depth/m	12
Annual mean precipitation/mm	700–850
Annual mean evaporation/mm	950
Annual mean relative humidity/%	70
Annual mean river runoff/m^3	15.97×10^8

The reservoir is one of the most highly monitored in Liaoning Province, with the historical data being monitored since 1975. The annual mean precipitation ranges from 700 mm to 850 mm and the annual mean evaporation is 950 mm (Table 1). The greatest amount of precipitation occurs during the summer, especially in July and August, accounting for approximately 47.6% of the annual amount, whereas during winter, only 3.4%–4% of the annual precipitation occurs. The annual mean river runoff is 15.97×10^8 m^3. Based on the statistics of historical data, Hunhe River provides 52.7% of the river runoff, followed

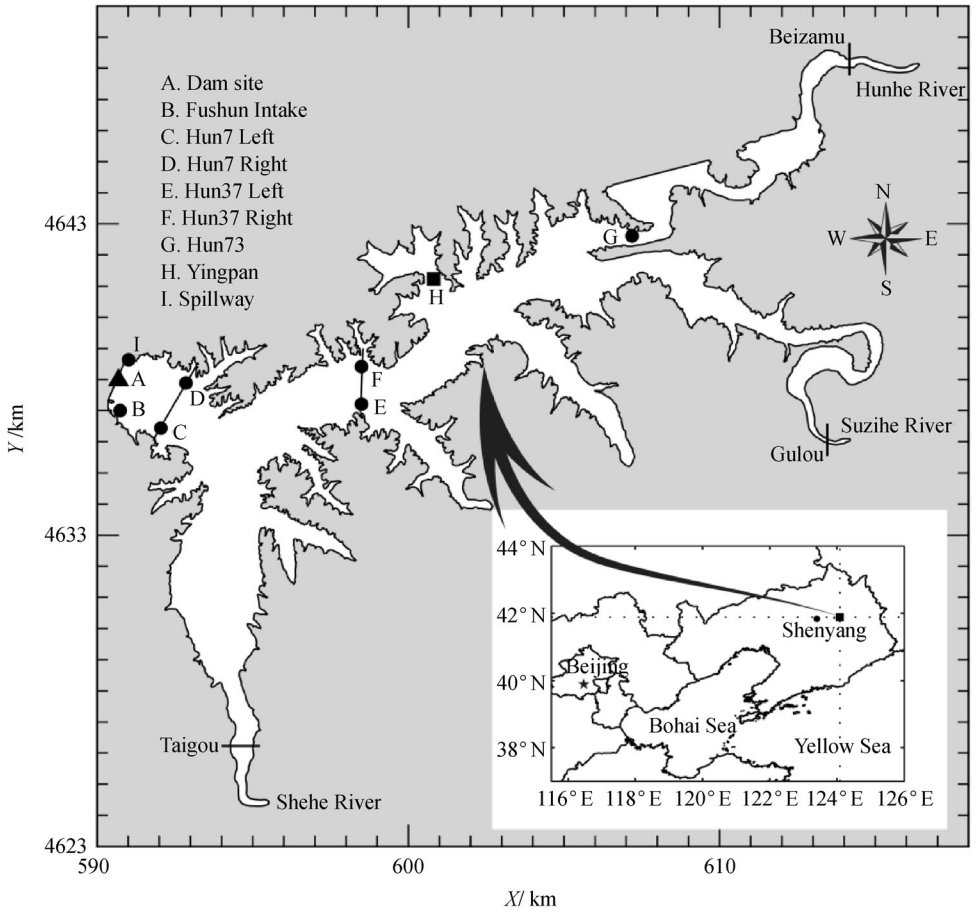

Fig. 1 Location and map of Dahuofang Reservoir. A, B, C, D, E, F, and G are the observation locations; H is Yingpan Station; I is the spillway.

by Suzihe River with 37.1% and Shehe River with 10.2%.

Flows into Dahuofang Reservoir show typical seasonality. Highest inflows occur from June through September. Lowest inflows occur in the remaining months (Shen et al., 2011; Wang et al., 2011). Additionally, flows into Dahuofang Reservoir can be categorized into two groups: point gauged and non-point distributed. Daily, point gauged flows were input to the reservoir at three survey stations, Beizamu, Gulou and Taigou (see Fig. 1), each being located at the upstream of Hunhe River, Suzihe River and Shehe River, respectively. The non-point distributed flows at undefined locations are not monitored, while they can be computed and pooled into the stations based on precipitation, evaporation, etc.

2.2 The numerical model

2.2.1 Description of the hydrodynamic model

A three-dimensional finite difference hydrodynamic and sediment transport model for shallow water environments – rivers, bays, estuaries, and the coastal ocean, reservoirs, and lakes, namely ECOMSED, was used in this study. The model was described in detail in Blumberg and Mellor (1987) and HydroQual Inc (2002), and therefore, only a brief outline is given here. The model resolves hydrodynamic equations which describe velocity, surface elevation, temperature, and salinity fields under two simplifying approximations: the hydrostatic assumption and the Boussinesq approximation. It incorporates the Mellor and Yamada level 2.5 turbulence closure scheme (Mellor and Yamada, 1982), which was modified by Galperin et al. (1988) and afterwards corrected by Mellor (2001), to characterize the turbulence by equations for the turbulence kinetic energy and a turbulence macroscale. The model uses an orthogonal curvilinear coordinate system in the horizontal plane and a terrain-following sigma-coordinate transformation in the vertical.

Mode splitting technique (Simons, 1974; Madala and Piacseki, 1977) is used in the model to permit the calculation of the free surface elevation with little sacrifice in computational time by solving the volume transport

separately from the vertical velocity shear. The prognostic variables are the three components of velocity, temperature, salinity, turbulence kinetic energy, turbulence macroscale, density, vertical eddy viscosity, and vertical eddy diffusivity. All variables are positioned on a staggered or "Arakawa-C" grid. The model formulation uses the finite control volume principle. The multidimensional positive definite advection transport algorithm (MPDATA), developed by Smolarkiewicz (1984), is applied. The subgrid scale processes not directly resolved in the model are parameterized in terms of horizontal mixing coefficients. ECOMSED calculates the horizontal diffusion according to the parameterization suggested by Smagorinsky (1963), which adjusts the scale of mixing to the grid size.

Three bulk formulae for computations of four major heat flux components, such as shortwave solar radiations, longwave atmospheric radiations, sensible heat fluxes, and latent heat fluxes, have been introduced in ECOMSED based on the works of Large and Pond (1982), Rosati and Miyakoda (1988), and Ahsan and Blumberg (1999). It has been demonstrated that the bulk formulae of Ahsan and Blumberg (1999) have more success in simulating heat budget in inland lakes, reservoirs, and estuarine systems.

Simulation of the transport of a dissolved tracer can also be accomplished using ECOMSED, with the tracer being either conservative or having a first-order decay rate. Temporally varying tracer concentrations can be easily specified for all boundaries and a tracer can be released from any location within the domain at any time.

ECOMSED has been successfully applied to many water bodies, such as estuaries, lakes, and coastal bays (Ahsan and Blumberg, 1999; Dabrowski and Hartnett, 2008; Hellweger and Masopust, 2008; Dabrowski and Berry, 2009; Ma et al., 2009; Robins and Elliott, 2009; Zhang and Zhang, 2011; Dabrowski et al., 2012). However, the standard release version of ECOMSED does not allow for simulation of the wetting and drying (WAD) changes of the grid cells in intertidal marshes, tidal flats, or flood plains. In the next section, a WAD scheme that can be easily imported into ECOMSED is introduced.

2.2.2 WAD scheme

WAD is a common and important phenomenon in reservoir operation due to the water level regulation for flood control, varying seasonal hydrological inputs, as well as power generation, etc. It is intrinsic for numerical model owning the capability of WAD to simulate hydrodynamics of a reservoir. A WAD scheme has been proposed and applied to the Princeton Ocean Model (POM) by Oey (2005, 2006). Moreover, the scheme which has been extensively tested on idealized one-, two-, and three-dimensional flows and then applied to real world scenarios (Oey et al., 2007; Blanton et al., 2010) appeared to be robust. Since ECOMSED shares POM's features: sigma-coordinate, time-splitting, and C-grid, the scheme can be easily imported into ECOMSED.

To implement WAD, an absolute land boundary (ALB), across which water can never flood, is initially defined. The datum of bathymetric depth H (non-negative (vertical) distance from the datum to the bottom topography) is lifted from the conventional definition for ocean models H_{msl} to $H_{\mathrm{msl}} + H_{\mathrm{hi}}$, where H_{msl} is the height from the bottom to mean sea level (msl), positive (negative) if the bottom is below (above) the msl, and H_{hi} is a constant height (>0). The water surface is then measured from the datum, which is $\eta(x, y, t) = {}^{-}H_{\mathrm{hi}} + \eta_{\mathrm{msl}}(x, y, t) \leqslant 0$, where $\eta_{\mathrm{msl}}(x, y, t)$ defines deviation of surface from the msl. The total water depth is then $D = H + \eta(x, y, t) = H_{\mathrm{msl}} + \eta_{\mathrm{msl}}(x, y, t)$. It is easy to figure that:

$$H \leqslant -\eta \text{ or } D \leqslant 0 \text{ if dry at any}(x,y,t), \tag{1}$$

and vice versa if wet.

The land-sea mask FSM is set to 0 at landward of ALB, but 1 at all other cells including potential WAD regions. A new separate time-dependent mask WETMASK, for the purpose of distinguishing between wet and dry cells, is then defined as:

$$\begin{aligned} \mathrm{WETMASK} &= 0 \text{ for } D \leqslant H_{\mathrm{dry}}, \\ &= 1 \text{ otherwise.} \end{aligned} \tag{2}$$

The $H_{\mathrm{dry}} = O(\mathrm{cm})$ is a pre-assigned depth for dry cells. It is useful to think of the dry cells as having a thin film of fluid with a thickness equaling H_{dry}. At each external time step, after η and the depth-averaged velocity (U, V) are updated, D is updated and Eq. (2) is applied. The final condition is that no fluxes across a dry cell-face can be imposed.

$$\begin{aligned} U_{i,j} &= 0 \text{ if } \quad (D_{i,j} + D_{i-1,j})/2 \leqslant H_{\mathrm{dry}} \\ V_{i,j} &= 0 \text{ if } \quad (D_{i,j} + D_{i,j-1})/2 \leqslant H_{\mathrm{dry}}, \end{aligned} \tag{3}$$

where i and j are the grid indices in the longitudinal and lateral directions. To enhance the robustness of the model, outflux from a dry cell must be shut off. Thus

$$\begin{aligned} U_{i,j} = 0 \text{ if } \mathrm{WETMASK}_{i-1,j} = 0 \text{ and } U_{i,j} > 0, \\ \text{or } \mathrm{WETMASK}_{i,j} = 0 \text{ and } U_{i,j} < 0. \\ V_{i,j} = 0 \text{ if } \mathrm{WETMASK}_{i,j-1} = 0 \text{ and } \mathrm{V}_{i,j} > 0, \\ \text{or } \mathrm{WETMASK}_{i,j} = 0 \text{ and } \mathrm{V}_{i,j} < 0. \end{aligned} \tag{4}$$

For the general three-dimensional baroclinic flows, two additional conditions and two auxiliary implementations are required. The first condition is that the temperature and salinity of the thin film of fluid in dry cells adjust to their surroundings:

$$\frac{\partial T}{\partial t} = -\alpha(T - T_a) \text{ if } \mathrm{WETMASK} = 0, \tag{5}$$

where T is the water temperature; t is the time; α is the relaxation coefficient, and 1 d^{-1} can then be used. A similar equation for salinity or other scalar transport materials can be easily extended. The second condition is that there can be no vertical (baroclinic) velocity structures across a dry cell-face:

$$u_{i,j,k} = U_{i,j} \text{ if } \text{WETMASK}_{i,j} \times \text{WETMASK}_{i-1,j} = 0,$$
and
$$v_{i,j,k} = V_{i,j} \text{ if } \text{WETMASK}_{i,j} \times \text{WETMASK}_{i,j-1} = 0 \quad (6)$$

where k is the vertical grid index, and u and v are the velocity components in the longitudinal and lateral directions. Two auxiliary implementations should also be imported: one deals with the way WETMASK should be defined to ensure consistency in external and internal mode integration; and the other concerns boundary conditions for the shear stress near the bottom when cells are drying and fluid becomes very thin. For details of the WAD scheme, see Oey (2006).

2.2.3 Residence time

The estimation of residence time has an important implication to the fates of introduced substances (Liu et al., 2012) and the primary productivity in aquatic systems (Wang et al., 2004). However, the precise definition of the term has varied over years and from one researcher to another; several researchers have remarked on this inconsistency, e.g., Zimmerman (1976), Takeoka (1984), Vallino and Hopkinson (1998) and Monsen et al. (2002). The definition of residence time by Zimmerman (1976), as the time a particle will spend in a defined region after first arriving at some starting location, was used in this study. Considering the amount of an introduced substance contained within a certain area in a reservoir at the initial time as M_0, and the amount of the substance remained in the reservoir at a given time as $M(t)$, the residence time distribution function of the substance can be expressed as:

$$\phi = -\frac{1}{M_0}\frac{\mathrm{d}M(t)}{\mathrm{d}t}. \quad (7)$$

$M(t)$ then is the amount of the substance whose residence time is greater than t. Thus, the average residence time is given by

$$\tau_r = \int_0^\infty t\phi(t)\mathrm{d}t. \quad (8)$$

It can be further assumed that

$$\lim_{t\to\infty} M(t) = 0. \quad (9)$$

Takeoka (1984) proposed the concept of remnant function:

$$r(t) = \frac{M(t)}{M_0}, \quad (10)$$

and by integrating Eq. (8) by parts arrives at:

$$\tau_r = \int_0^\infty r(t)\mathrm{d}t. \quad (11)$$

It is clearly shown that calculations are easily achieved for determining the residence time for a material element that is discharged into a body of water at a particular location and time when the remnant function of the pollutant is obtained.

For a reservoir of constant volume, the mass of the material in Eqs. (7), (9), and (10) can be replaced with its concentration. It is also easily shown that in a well-mixed body of water, τ_r equals the e-folding time (van de Kreeke, 1983), τ_e, which is the time required to reduce the initial mass of an instantaneous injection of a tracer by a factor of e. This suggests a possible characterization of flushing time scales in non-CSTR (completely stirred tank reactor) systems as the e-folding time (Rueda et al., 2006). In this study, we treat individual numerical model's cells as completely mixed reactors; therefore, we calculate the e-folding time, τ_e, of each cell to compute the spatial distribution of residence time. A similar method was used in previous works (Dabrowski and Berry, 2009; Dabrowski et al., 2012).

3 Model configuration and validation

3.1 Model configuration

The model domain covers the entire reservoir and up to Beizamu, Gulou, and Taigou, upstream from Hunhe River, Suzihe River, and Shehe River, respectively. It is difficult to design a body-fitted grid for such an irregular domain (Fig. 1) as Dahuofang Reservoir; thus, a simple rectangular grid with a resolution of 100 m was constructed. The vertical 6 sigma levels were unevenly distributed, which resulted in a vertical resolution of about 0.04−1 m in the regions that are shallower than 5 m and about 7 m at the 35 m isobath. In total, 264×246 horizontal grid cells and 5 sigma layers were defined in the model domain. The bathymetry on the model grid was interpolated by the distance weighted interpolation method from the field observation data, which was collected by the Department of the Dahuofang Administration Bureau (DDAB) and Liaoning Academy of Environmental Sciences (LAES). The interpolated bottom topography of Dahuofang Reservoir is shown in Fig. 2.

There are three river inflows and two withdrawals (Fig. 1) in the model domain. The discharges and water temperature of the inflows and withdrawals were provided through the field observations. Figure 3 shows these daily

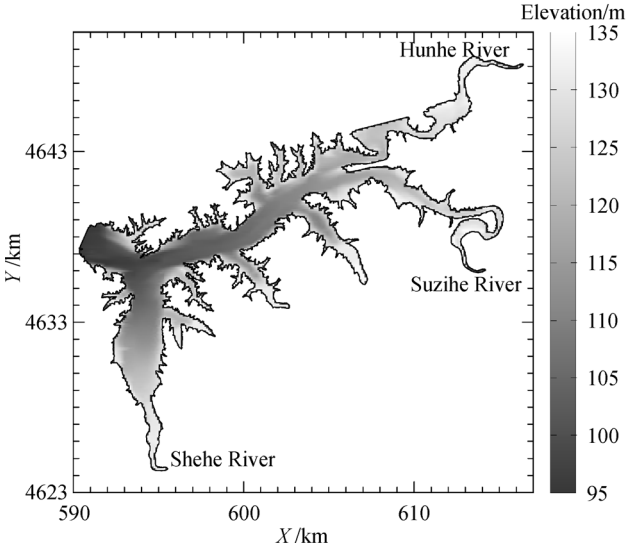

Fig. 2 Bottom topography of Dahuofang Reservoir

discharges. The total inflow as seen in Fig. 3 was calculated by DDAB based on the water level at the dam site, and the outflow and water loss of the reservoir, which means that precipitation, evaporation, seepage, and other distributed flows were involved. The difference of the total inflow and the sum of the river inflows were proportionally assigned to the three rivers in the model simulation. At the free surface, meteorological parameters, such as wind components at 10 m above the water level, downward shortwave radiation, air temperature, relative humidity, barometric pressure, cloud cover fraction, precipitation, and evaporation, were provided to calculate the wind stress and heat fluxes. These parameters were obtained from the 3-hourly reanalysis of ERA-Interim, maintained by European Centre for Medium-Range Weather Forecasts (ECMWF), except for the precipitation and evaporation which were obtained at daily intervals from the field observations at Yingpan Station. Some meteorological parameters are shown in Fig. 4 at 06:00 UTC each day from April 1st to November 30th, 2008. As far as bottom roughness was concerned, the value of the friction coefficient was set to 0.0025 and the roughness height z_0 to 0.01 m. On the sidewalls and bottom of the reservoir, the normal gradients of temperature were zero so that there were no advective and diffusive heat fluxes across these boundaries. The horizontal Prandtl number, defined as the ratio of horizontal viscosity to horizontal diffusivity, was held constant and set equal to the recommended value of 1.0 (HydroQual Inc, 2002). The value of the Smagorinsky coefficient was fixed to 0.1. The background vertical mixing parameter in Mellor and Yamada's turbulence closure scheme (Mellor and Yamada, 1982) was specified as $1.0\times10^{-6}\,\mathrm{m^2\cdot s^{-1}}$ (HydroQual Inc, 2002). The vertical Prandtl number, defined as the ratio of vertical viscosity to vertical diffusivity, was held constant and set equal to the recommended value of 1.0 (HydroQual Inc, 2002). The wind sheltering coefficient was set to 0.85. The fraction of short wave radiation absorbed in the surface layer was calibrated as 0.45 and the extinction coefficient as $0.45\ \mathrm{m^{-1}}$.

The initial water temperature was assumed uniformly distributed in the entire model domain and equaled to the observed temperature at the dam site. The initial water level and current were set to zero. The threshold for cells transiting from wet to dry was set to 0.2 m, and the isobath of 140 m was set as the ALB, which means that H_{dry} = 0.2 m and H_{hi} = 8.5 m. When applying the WAD scheme in real-world circumstances, it is believed that a smaller time step than that decided by Courant-Friedrichs-Lewy (CFL) condition is needed (Oey et al., 2007). For computational accuracy and efficiency, a series of tests was made to determine the appropriate time steps. Finally, external mode time step of 0.75 s, and internal mode time step of 20

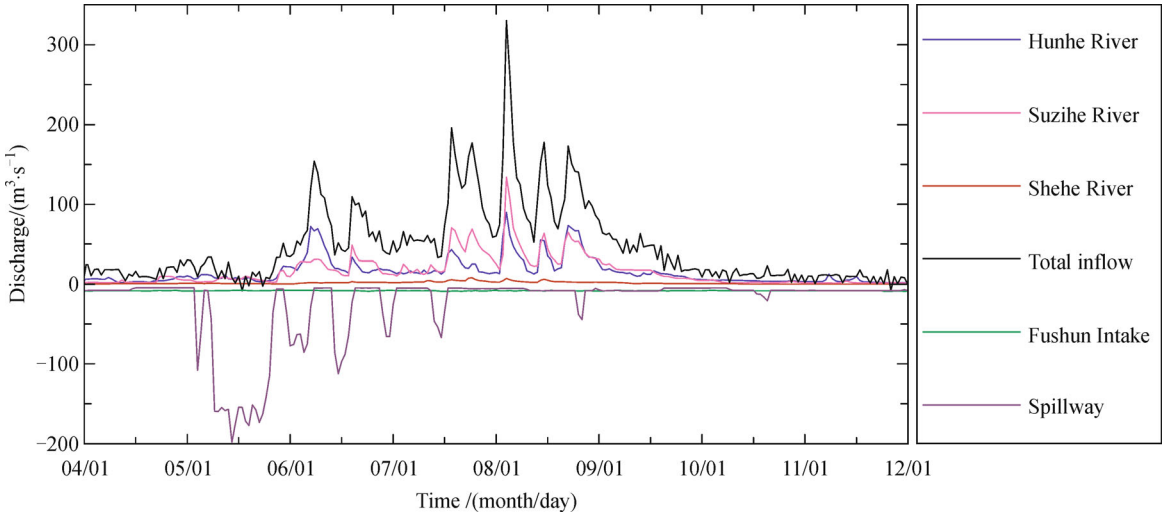

Fig. 3 Inflows and withdrawals hydrograph of Dahuofang Reservoir

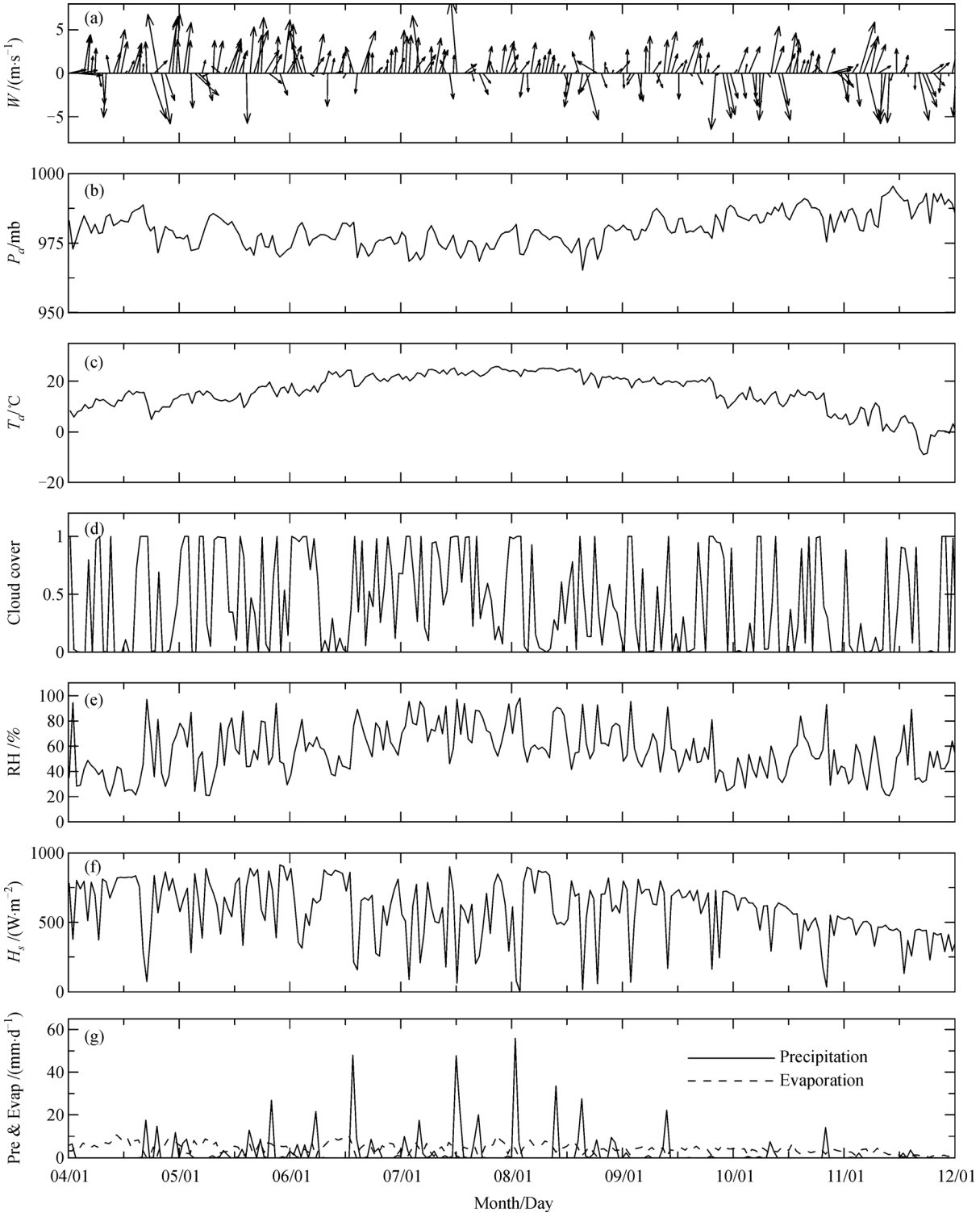

Fig. 4 Meteorological parameters of Dahuofang Reservoir from April 1st to November 30th, 2008 at 06:00 UTC each day. (a) 10 m high wind speed; (b) barometric pressure; (c) air temperature; (d) cloud fraction; (e) relative humidity; (f) downward shortwave radiation flux; (g) precipitation and evaporation at Yingpan Station

times that of the external mode were chosen. The simulation was started on February 1st, 2008, and ended on November 30th, 2008. The prior two months of the simulation were used to spin up the model, and the results of other months were analyzed and presented.

3.2 Model validation

3.2.1 Water elevation

The observed data of water surface elevation collected from April 1st to November 30th, 2008 at the dam site was used to verify the performance of the model. Figure 5 presents the comparison of model-calculated surface elevation and the observed elevation at Station A. In general, the model consistently reproduced the water level variation throughout the year. The root mean squared error (RMSE) and the mean absolute error (MAE) between the simulated results and the observed free-surface elevation are 0.459 m and 0.372 m, respectively. It is to be noted that the model captured the sharp water level fluctuation utilizing a year-round reservoir observation. The figure also provides a validation for the successful implementation of the WAD scheme described in Section 2.2.2. The good comparison of water elevation implies that the hydrodynamic model was correctly set up and was suitable for determination of the water flushing properties of the reservoir.

3.2.2 Water temperature

Water temperature in a reservoir is affected by meteorological conditions, river inflows and withdrawals, density circulation, as well as turbulent mixing processes. Therefore, the water temperature distribution reflects the combined result of all the processes, and in turn, it controls density circulation and modifies mixing processes. In the present study, the time series of water temperature collected from field observations were adopted for model validation. Figure 6 shows the comparison of modeled and observed water temperature at seven stations. Water temperatures were measured for the surface layer at Stations A and G and for the middle layer at Station B. The counterparts of the model layers at these stations were thus displayed.

At all the stations, the simulated surface temperature matches the observed data favorably well. The modeled temperature of the middle layer of Station B agrees closely with the observed data except for August. This discrepancy should be attributed to the inconsistencies in the elevation at which the field observation was carried out and at which the model calculated the water temperature. In actuality, Station B, Fushun Intake, must be fixed to a specific elevation, but varied with the change in water level during the simulation due to the sigma representation of ECOMSED in the vertical. In August, even though the water level of the reservoir was gradually ascending (Fig. 5), the elevation of the middle layer of Station B in the model was still lower than its actual value. Thus the modeled water temperature was lower than the observed temperature. The temperature of the bottom layer is also in good agreement with field observations, especially at Station C. The disagreement at other stations can be ascribed to the equally distributed extinction coefficient used for calculating heat budgets in the reservoir and imprecise representation of the bathymetry. It is believed that the accuracy of the model could be improved if more precise field observations could be provided. In summation, the comparisons show a good agreement between the modeled and observed water temperature at each station.

A vertical profile of the calculated temperature at Station A over a period of eight months in 2008 is shown in Fig. 7. It can be seen from the figure that the thermal stratification

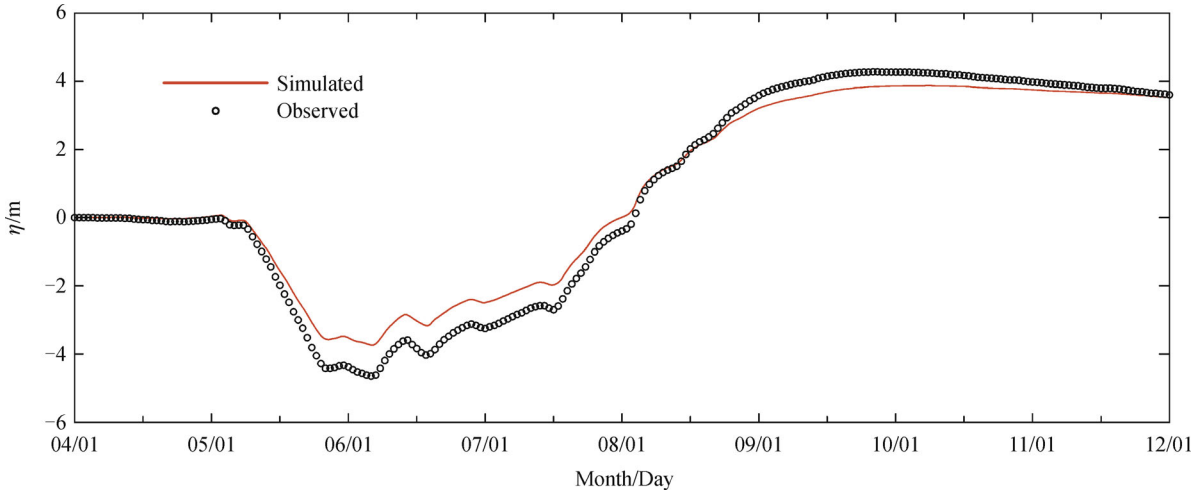

Fig. 5 Comparison between simulated (solid line) and observed (circle) time series of water surface elevation at Station A

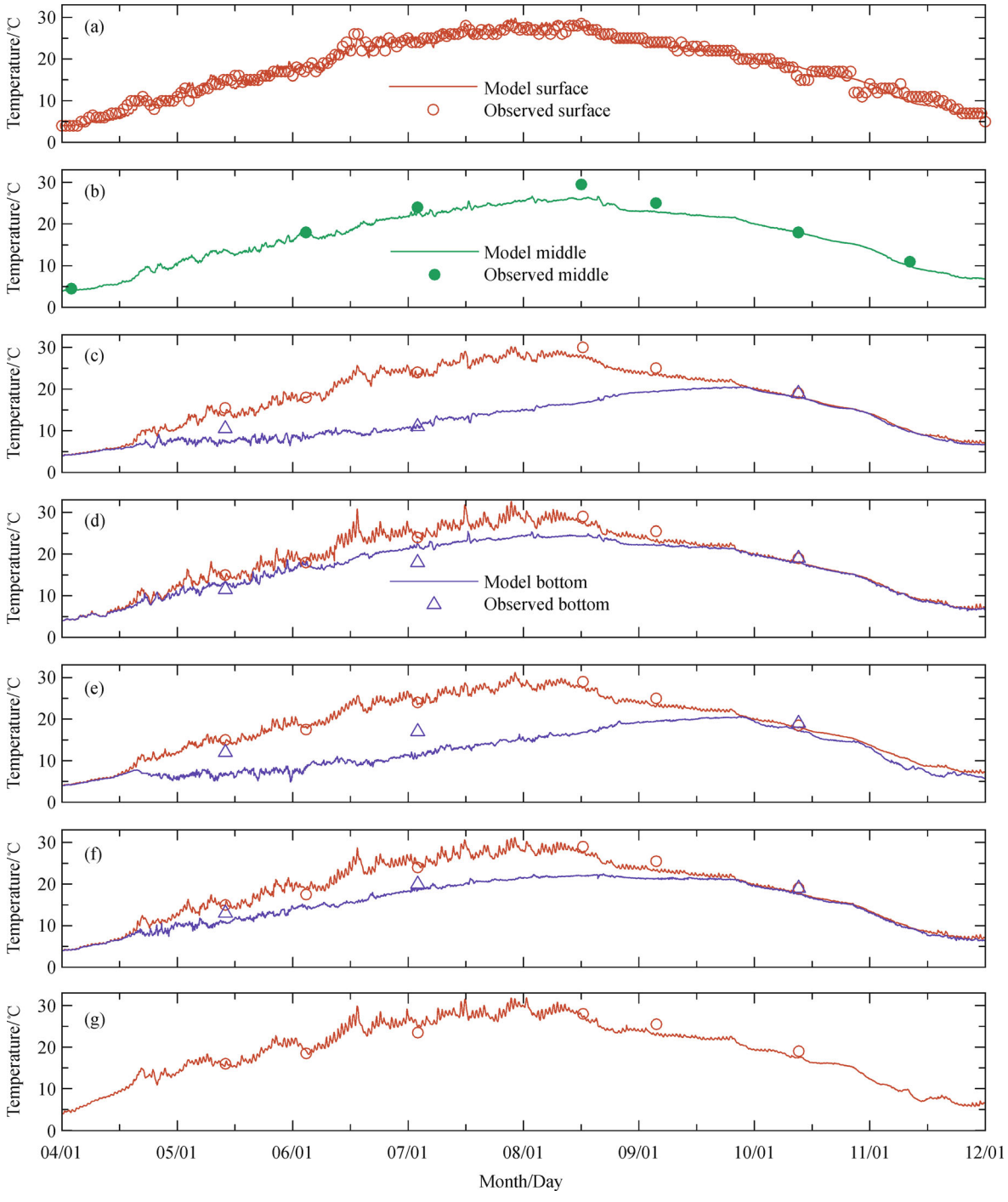

Fig. 6 Comparison between modeled and observed time series of water temperature at Station (a) A, (b) B, (c) C, (d) D, (e) E, (f) F, and (g) G

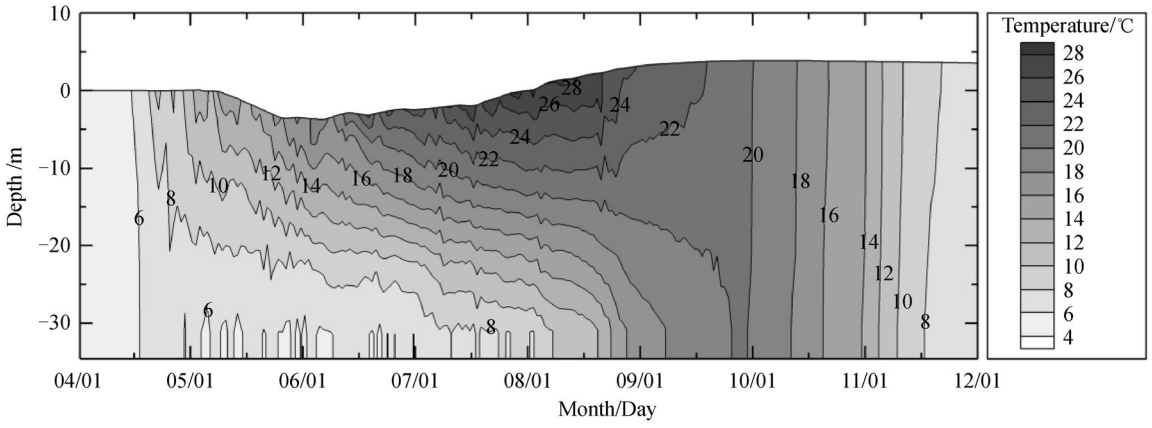

Fig. 7 The vertical thermal structure from April to November of 2008 at Station A

started in early May, the beginning of spring, and concluded at the end of September because of surface cooling and wind-induced mixing. The stratification reached its maximum during the summer. In the stretches of the model run, the maximum temperature difference between the surface and bottom layers at Station A was 20.8 °C, and occurred in late July. Figure 8 shows a snapshot of the difference between surface and near-bed temperature on July 1st, as predicted by the model. The model predicted very strong thermal stratification in the reservoir in summer. It is interesting that Fig. 8 looks very similar to the topography of the reservoir (Fig. 2), as the heat fluxes calculated in the model run were based on spatially invariant meteorological parameters. For enhanced model accuracy, accurate, local meteorological observations are required.

The figures above demonstrate that the annual water temperature cycle was successfully reproduced by the model, and the vertical thermal stratification was also accurately modeled. Furthermore, these figures indicate that the model responded correctly to the major forcing functions: spring warming, fall cooling, and wind-induced mixing, and that it can be applied to determine the water flushing properties of the reservoir.

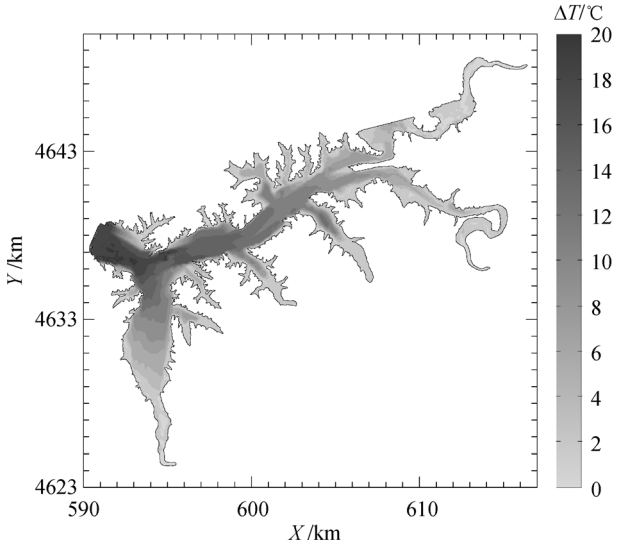

Fig. 8 Model-predicted surface-near-bed temperature difference on July 1st

4 Results and discussion

4.1 Calculation of the residence time

To determine the water flushing characteristics of Dahuofang Reservoir, a series of passive conservative pulse tracer release experiments was conducted. The simulations were to track the temporal evolution and spatial distribution of the tracer following its initial uniform distribution throughout the model domain. They were conducted not only to determine the residence time, but also to investigate the relative contribution to the flushing by each of the three major physical transport mechanisms: (1) inflows and withdrawals, (2) wind, and (3) density induced circulation. Four numerical experiments were conducted using the validated model to identify the prevailing influencing functions and the residence time distribution features: (1) the benchmark experiment with full forcing (EXP1); (2) a baroclinic experiment initialized as in EXP1, but without wind forcing (EXP2); (3) an experiment initialized as in EXP1, but without surface heat fluxes forcing (EXP3); and (4) a barotropic experiment forced only with inflows and withdrawals (EXP4). The differences between the control run and the experimental runs (EXP2 and EXP3) were used to investigate the effects of wind and heat fluxes, respectively, on residence time distribution of Dahuofang Reservoir. A comparison of EXP4 and EXP2 shows the baroclinic effect, while the comparison between EXP4 and EXP1 shows how the flows (including inflows and withdrawals) only influence the residence time distribution of Dahuofang Reservoir.

Eight flushing simulations in each experiment were carried out. The simulations differed in the tracer release time by releasing on the first day of each month from April to November, 2008. Changing the release time allows for assessment of the temporal dependence of the water flushing properties of the reservoir. The spatial distribution of the residence time was obtained by calculating the *e*-folding time of each computational cell as described in Section 2.2.3.

To run the tracer transport simulations, the model was forced with daily hydrologic records and three hourly meteorological parameters collected in 2008 as shown in Fig. 3 and Fig. 4. For computational efficiency, the hydrodynamic field of the year was first stored every 30 minutes to the disk and was then read to calculate the tracer transportation. The records were stacked to create a synthetic three-year time series. Nevertheless, for each simulation, the model was run for two years (732 days) after the tracers were released. The purpose for the multi-year simulation is to guarantee sufficient transport time for the tracer concentration in the computational cells to be less than e^{-1} of the initial. The model is ice free, which means that in the model runs, the reservoir's surface water cannot be frozen in winter. For simplicity, water temperature in winter was held to 4°C and was liberated in spring. The tracer was introduced to the model in the form of an instantaneous release and was uniformly dispersed throughout the model domain with concentration of 1 $mg \cdot L^{-1}$.

4.2 Water flushing characteristics of the reservoir

Since most natural reservoirs are not spatially well-mixed, the residence time varies dependent on location. Depending on the degree of mixing, the values of local residence time may significantly depart from the average value (Dabrowski and Berry, 2009). Shen et al. (2011) examined the residence time distribution of Dahuofang Reservoir by dividing the reservoir into seven segments. In this study, local residence time determined by τ_e (a 63% decrease in tracer concentration in a given cell) was calculated for each computational cell with the spatial distribution derived from the eight simulations in EXP1 plotted in Fig. 9. It should be noted that the depth averaged value of local residence time is displayed in each panel of Fig. 9. It can thus be concluded that the local residence time is highly spatially variable.

As for the entire domain of Dahuofang Reservoir, tracers in the Hunhe River and Suzihe River channels were flushed initially due to their predominant runoffs, and as a result, the local residence time in these two regions is short. However, tracers in the downstream of Shehe River would reside for a longer period of time, and thus, the local residence time in this area was determined to be the longest. For a better explanation, the depth averaged flow field in June and October, when the water elevation reached the lowest and the highest, respectively, was drawn for every other cell in Fig. 10. It can be seen from Fig. 10 that some circulations exist in the reservoir, especially in the downstream of Shehe River. The circulation combined with the weak runoff of Shehe River resulted in the long local residence time. A strong gradient of local residence time exists near the eastern bank of Shehe River, which could be ascribed to the weak northward river flow, the strong backwater, and the wide river span. Tracers in the branch streams took longer to reach the outlet than those in the adjacent reservoir areas. However, a strong local residence time gradient can also be found at the end of the branch streams. By contrasting Fig. 9 with Fig. 10, it can be obtained that the areas with low local residence time in the branch streams just coincide with the areas where the bottom was exposed to the air in June (Fig. 10(a)), while covered with water in October (Fig. 10(b)). Tracers no longer exist in these areas once they dry out. However, in the adjacent wet areas, the tracer may still exist with a higher concentration and would need a more time to decline to 0.37 $mg \cdot L^{-1}$. Thus, the strong gradient of local residence time is formed. The local residence time of the northern part of the reservoir is shorter than that of the southern part likely due to the existence of Coriolis force and asymmetry of bottom topography. In all simulations, local residence time at the head of the reservoir is almost equally distributed yet is less at the tail of the reservoir.

The local residence time is highly temporally variable, as shown in Fig. 9. Due to the increase of withdrawal in May (see Fig. 3), local residence time in most parts of the reservoir in R5 (Fig. 9(b)) is shorter than in R4 (Fig. 9(a)). In the rainy season (June−August), river runoff of Hunhe River and Suzihe River increased considerably (Fig. 3) due to abundant precipitation. Tracers released in the Hunhe River and Suzihe River channels and their confluence areas were soon flushed away, which resulted in low local residence time in these regions. The area of low local residence time (< 50 d) reaches the maximum in R7 (Fig. 9(d)). However, the local residence time in the downstream of Shehe River and at the head of the reservoir in R7 increased rapidly to over 320 d, which contrasts sharply to that in R4, R5, and R6. In R8, the long local residence time region extended to the middle part of the reservoir. In all the aforementioned five runs, the end of the branch streams was to be dry in less than 40 days or was dry at the initial tracer release time, which resulted in a short local residence time and hence, an obvious front of local residence time in the streams.

Two factors should be noted here. One is the short local residence time of R6 (Fig. 9(c)). After the tracer was released on June 1st, the water elevation gradually increased (Fig. 5) with an abundant amount of water stored in the reservoir. The newly stored water diluted the tracer and forced a quick decline in concentration reaching the threshold of 0.37 $mg \cdot L^{-1}$ for determining the local

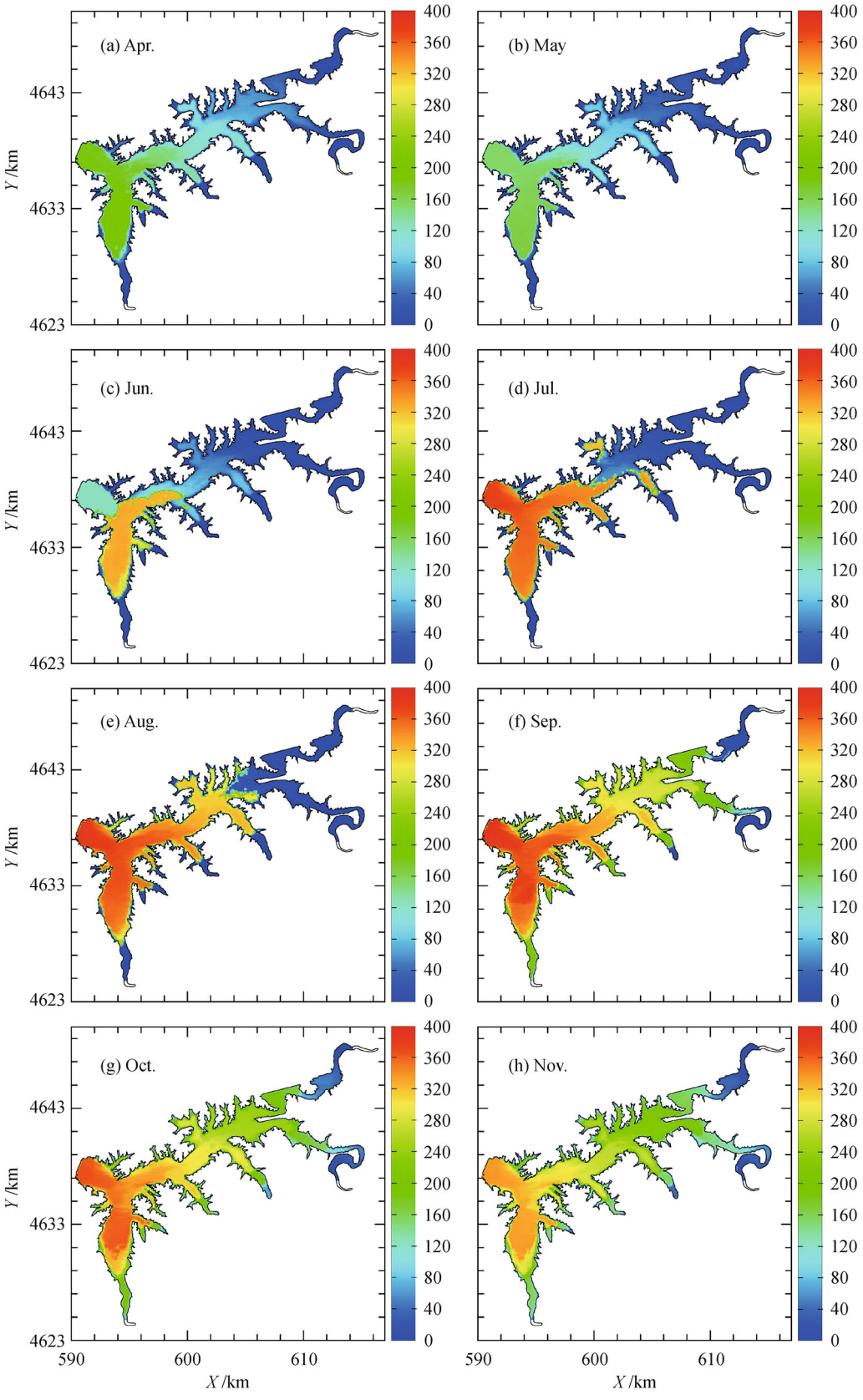

Fig. 9 The spatial distribution of local residence time (in days) of Dahuofang Reservoir under full real forcing functions (EXP1) for tracers released at the beginning of (a) April, (b) May, (c) June, (d) July, (e) August, (f) September, (g) October, and (h) November of year 2008

residence time. The second is the strong gradient of local residence time in the middle part of the reservoir developed in R7 and R8 (Fig. 9(d) and (e)). Even though the inflows were considerably large in July and August, the withdrawal was far less (Fig. 3) because of the reservoir operation for water storage in preparation for the coming dry season. The consequences of water storage include an increase in the water level, back flow towards the tail of the reservoir, etc. The back flow carries the tracer back and therefore increases the tracer concentration of the influenced regions. Thus it will take a long time for the tracer concentration of the cells in these regions to decline to $0.37\,mg\cdot L^{-1}$. However, in regions influenced more by river runoff, the time is short. Moreover, the value of local residence time is determined by the first time the tracer concentration reaches $0.37\,mg\cdot L^{-1}$. Thus, a front is formed in the middle part of the reservoir.

In R9, R10, and R11 (Figs. 9(f)−(h)), the local residence time in the tail of the reservoir, including streams of Hunhe River and Suzihe River and their confluence areas, increases in comparison to that in R8. This can partially be attributed to the slower current (Fig. 10), which prohibits the tracer from being flushed away as soon as that in R8. Generally, the local residence time in R9 is longer than that in R8. Although both the simulations of R8 and R9 experienced the entire water elevation down-up cycle, the influx of fresh water in R9 could not increase the water volume of the reservoir to dilute the tracer. The tracer amount decrease is fundamentally affected by the water withdrawal after the tracer was released. Therefore, even by using the same amount of time, the tracer amount in R9 did not decrease much more than that in R8, owing to the small withdrawal after August (Fig. 3). Thus, the combination of these factors resulted in the long local residence time in R9. At the initial time of tracer release in R9, R10, and R11, the entire bottom of the reservoir was covered with water. As time went on, some areas of the branch streams gradually became dry. The local residence time of these regions was then determined by the amount of time elapsed for the transition from wet to dry in case the tracer concentration was still higher than $0.37\,mg\cdot L^{-1}$ at the time the regions became dry. As a result, low local residence time regions are presented in these branch streams in R9, R10, and R11. In most areas of the reservoir, the local residence time shown in R9, R10, and R11 declined one by one, but maintained the same distribution pattern.

As was stated in Section 4.1, simulations were conducted by instantaneously introducing tracers uniformly throughout the model domain, then river runoff with no tracer was discharged into the reservoir. Since the flushing factor is the riverine water, the locations featuring the highest residence times are the slowest to respond to changing pollutant loadings (Dabrowski and Berry, 2009). The results of this study demonstrate that the activation of water supply safety management in case a pollution accident occurs is within a sufficient timeframe, due to the responding speed of Fushun Intake to a pollutant discharged at the upstream is much slow. Phytoplankton bloom is more likely to occur in July, August, and September when the water temperature is adequate for promoting phytoplankton growth and the longer residence time of the water allows for nutrients to reside in the water column.

It should be noted that the results obtained in this paper are based on the hydrological and meteorological conditions in 2008. To derive more general conclusions, it is recommended that hydrological and meteorological conditions representing a typical year are used for the model forcing. It should also be noted that the methodology presented in this paper is based on general water circulation (with a conservative tracer used as the indicator of transport and mixing processes in the reservoir) rather than being pollutant specific.

4.3 Factors that control water flushing

It is well known that the physical processes of transport and mixing of a reservoir's content are mainly affected by its shape and hydrological and meteorological conditions. Even though reservoir shape remains stable and specific for each, a variance in influence factors occurs over time, including the inflows and withdrawals, wind, and heat fluxes. The heat exchange with the atmosphere causes water temperature in the reservoir to rise and fall seasonally and establishes thermal stratification during the warm season if a reservoir is sufficiently deep. A vertical water exchange is difficult due to the stable density gradient aroused by thermal stratification. In nearly all lakes, wind is the decisive factor for the thickness of the epilimnion (Boehrer and Schultze, 2008). The kinetic energy input through wind stress at the surface facilitates a much more efficient heat transport. The stronger the wind, the deeper the surface water was pushed down. A review of the physical processes that occur within lakes or reservoirs has been presented and discussed in Imberger and Patterson (1989) and Boehrer and Schultze (2008).

To investigate the influences of inflows and withdrawals, wind, and heat fluxes on the water flushing properties of Dahuofang Reservoir, experiments were designed as discussed in Section 4.1. Each experiment includes eight tracer release simulations in which the tracer was initially uniformly distributed and released at the beginning of the eight months (April−November) of 2008. The local residence time distribution of R7 and R11 when the tracer was released on July 1st and November 1st was displayed as the representative and is shown in Fig. 11 and Fig. 12, respectively. The purpose for selecting R7 and R11 is that in July, both the inflows and withdrawals (Fig. 3) and the thermal stratification (Fig. 8) were strong. Additionally, in November the reservoir operated at a high water level with little variability (Fig. 5) and there was no thermal

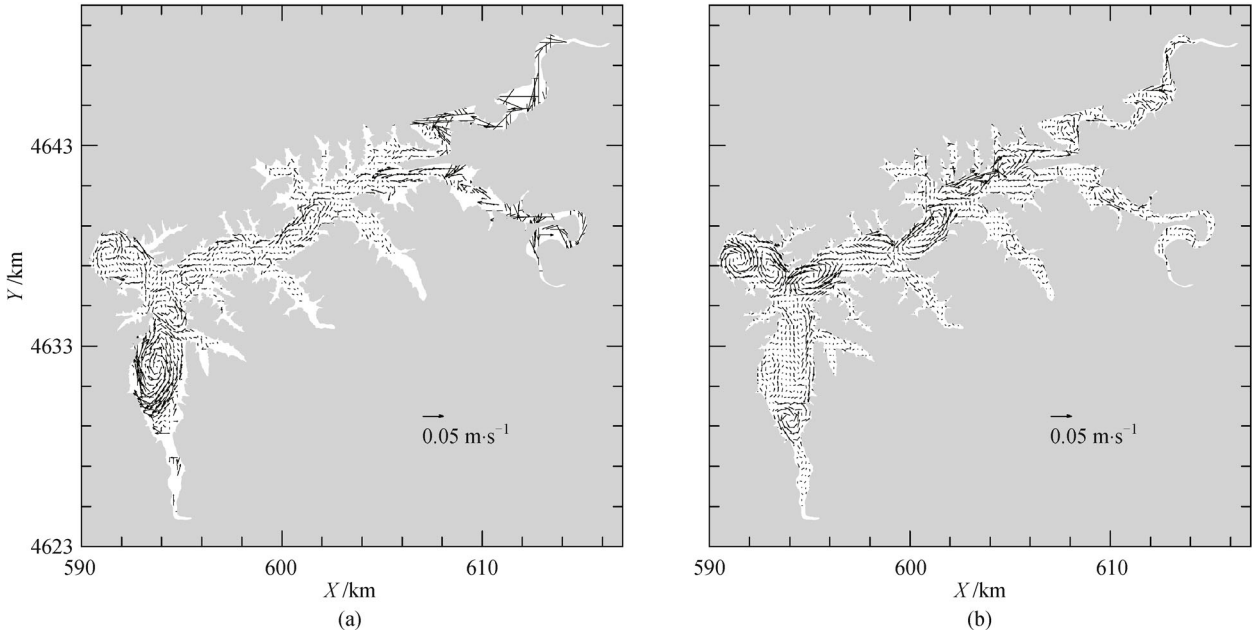

Fig. 10 Flow field of Dahuofang Reserovir on (a) June 1st, 2008 and (b) October 1st, 2008 in EXP1

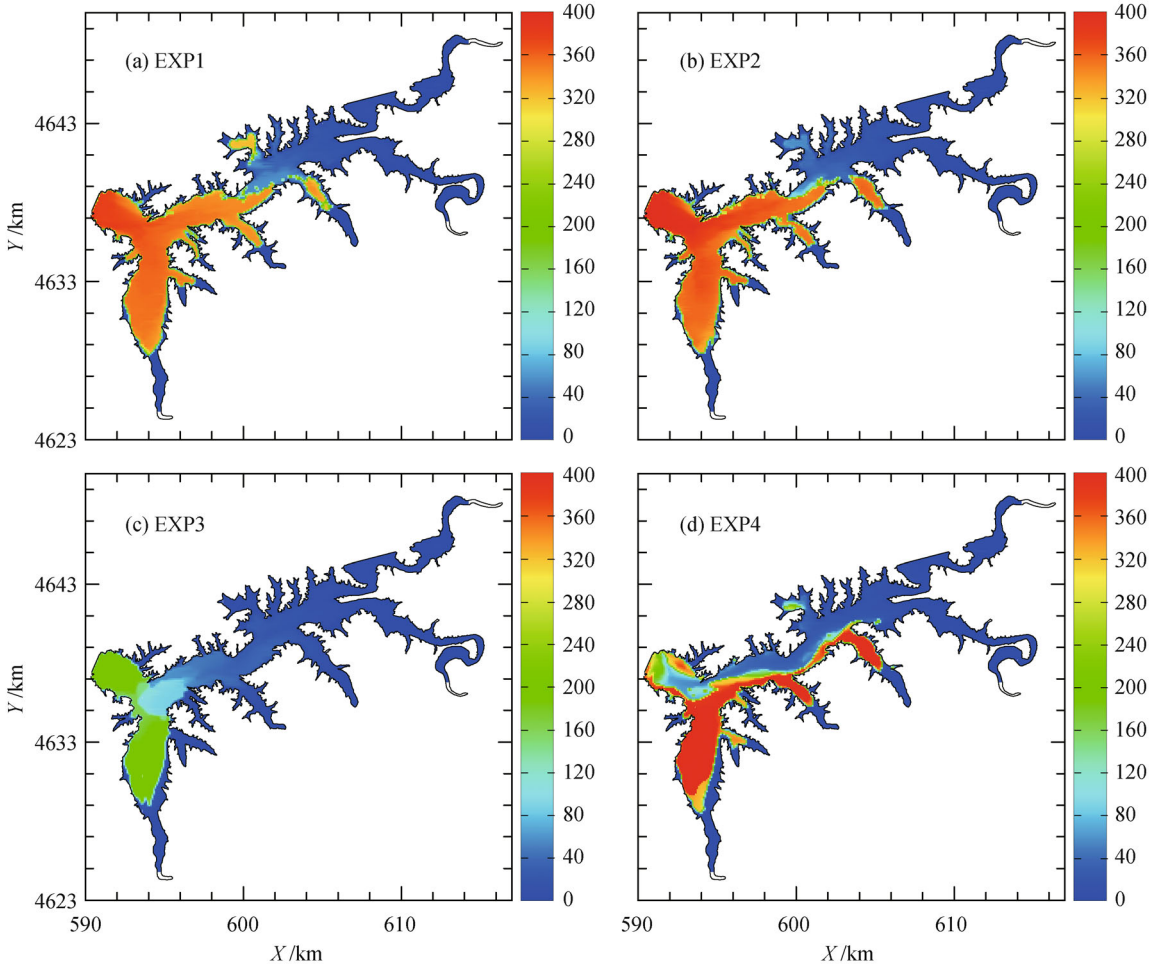

Fig. 11 Comparison of the spatial distribution of local residence time (in days) of Dahuofang Reservoir for tracers released on July 1st in the four experiments designed in Section 4.1

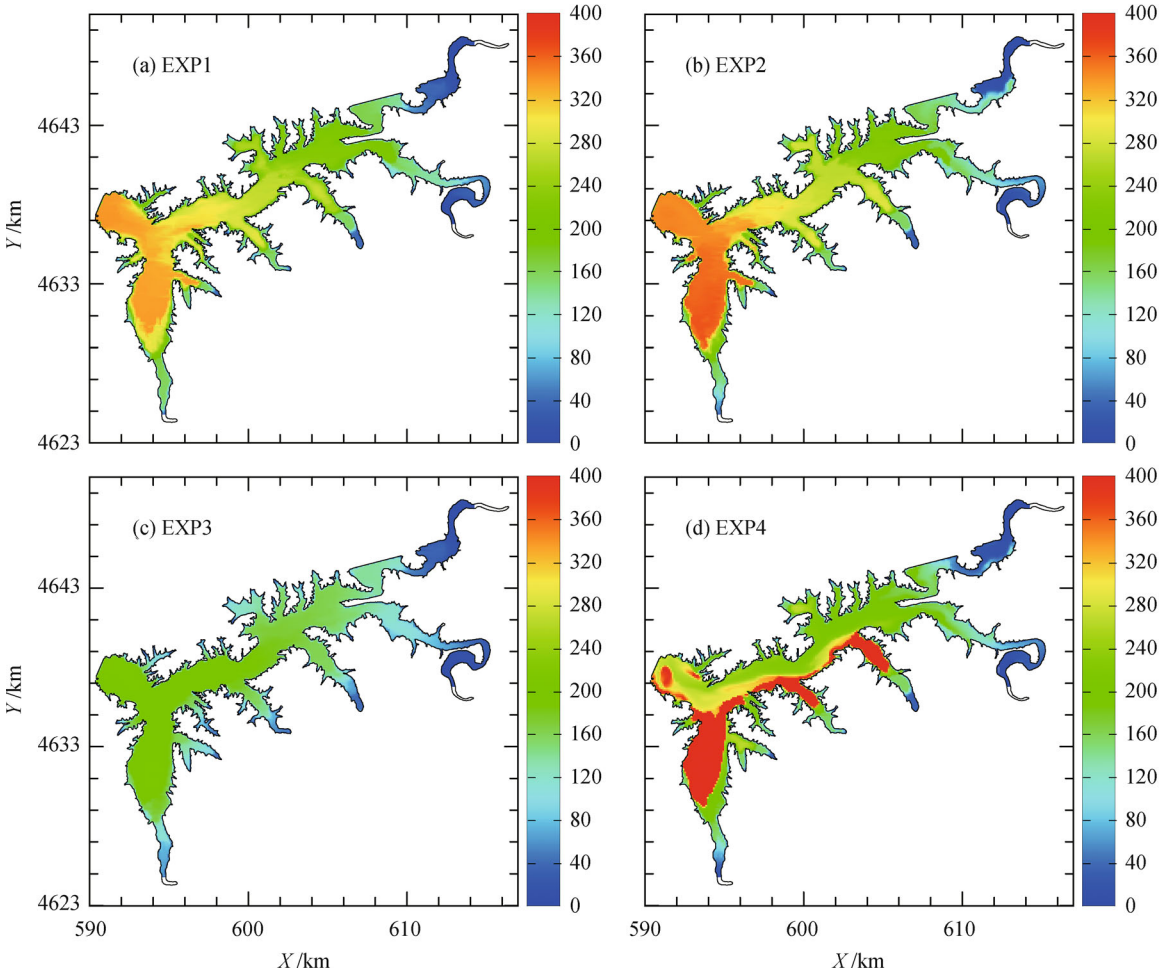

Fig. 12 Comparison of the spatial distribution of local residence time (in days) of Dahuofang Reservoir for tracers released on November 1st in the four experiments designed in Section 4.1

stratification (Fig. 7). It should be noted that the local residence time shown in Fig. 11 and Fig. 12 is vertically averaged.

The distribution patterns of the local residence time in EXP1 and EXP2 for R7 and R11 show some similarity with only slight differences, which can be obtained from the comparison between Fig. 11(a) and (b) and Fig. 12(a) and (b). First, the value of local residence time in most areas of the reservoir increased when wind was not taken into consideration. Secondly, the local residence time of the branch stream where Yingpan Station is located decreased in R7 in EXP2. Thirdly, the local residence time near section Hun37 is more disturbed in EXP2. The model predicted a strong thermal stratification in summer, so the tracer in deep water was to reside for several months until the stratification became weak or vanished. Wind can deepen the depth of epilimnion and make the stratification vanish quickly. Therefore, it is clear why the local residence time of the reservoir in EXP2 is larger than that in EXP1. In summation, wind is an important influencing factor for determining the water flushing of Dahuofang Reservoir.

In the runs of EXP3, with flows and wind being considered, the local residence time for R7 (Fig. 11(c) and Fig. 12(c)) is far less than for R11 (Fig. 11(a) and Fig. 12(a)), especially in the downstream of Shehe River and the head of the reservoir where water is deep. The comparison implies that the thermal stratification established in Dahuofang Reservoir is so strong that the tracer transport and mixing in the vertical were severely limited. The comparison of local residence time demonstrates that heat fluxes have a stronger effect than the wind on the water flushing of Dahuofang Reservoir.

The residence time distribution pattern of EXP4 differs markedly from that of EXP2, which can be obtained from the comparison between Fig. 11(d), Fig. 12(d) and Fig. 11 (b), Fig. 12(b). Water temperature in shallow regions always responds to climate change faster than that in deep regions. Thus, a density difference exists between the shallow branch streams and the deep main reservoir. The density driven flow strengthens the advection between the main reservoir and the branch streams and distributes the

local residence time more evenly (Fig. 11(b) and Fig. 12 (b)). On the other hand, thermal stratification caused by the heat fluxes restricts mixing in the vertical direction and prolongs the time for tracers to leave the reservoir. From the comparisons between EXP1 and EXP3 and between EXP4 and EXP2, it can be concluded that heat fluxes are the controlling factors of the water flushing of Dahuofang Reservoir.

When considering the flows only (EXP4), there is a significant variation in the spatial distribution of local residence time (Fig. 11(a) and 11(d) and Fig. 12(a) and 12 (d)). Tracers in the deep water channel of the reservoir were flushed away quickly, thus limiting the time they resided in the channel. However, the tracers in the branch streams, specifically those on the southern bank of the reservoir, were squeezed by the strong currents in the deep water channel preventing them from flushing out, thus increasing the local residence time in these regions to extremely high levels. When taken wind and heat fluxes into consideration (EXP2), the tracers on the eastern bank of Shehe River flushed slower and nearer. It can then be derived that the inflows and withdrawals are the decisive factors of water flushing.

5 Conclusions

A three-dimensional hydrodynamic model with the capability to deal with changing land water boundaries was developed based on ECOMSED in this study. It was then configured for Dahuofang Reservoir to numerically study its water flushing characteristics. The configuration was validated with field observation data of water surface elevation and water temperature in 2008. The intra-annual water level fluctuation was well reproduced, and the simulated and observed water surface elevation matches closely with the RMSE equaling 0.459 m at the dam site. Furthermore, the temporal evolution and spatial distribution of water temperature were nicely reproduced and the comparisons between the simulated and observed temperature in the water column show a good agreement.

Residence time is a parameter used for describing the capability of a water body to renew its water contents and can aid in the assessment of the environmental status of the water body. In this study, a series of numerical modeling experiments for better understanding the water flushing characteristics of Dahuofang Reservoir was conducted based on the previously validated model. The general conclusions derived from the experiments can be summarized as follows:

1) The water flushing of Dahuofang Reservoir is highly temporally variable. The distribution pattern of local residence time in simulations with different tracer releasing times varies from one to another (Fig. 9). The area with low local residence time (< 50 d) reaches the maximum in R7, while the area with high local residence time increases rapidly as well in R7. Phytoplankton bloom is more likely to occur in July, August, and September due to the appropriate water temperature and the long local residence time of the reservoir during these times.

2) The water flushing of Dahuofang Reservoir is highly spatially variable. The shortest local residence time occurs in the channels of the Hunhe and Suzihe Rivers due to their predominant runoffs, while the longest occurs in the downstream of Shehe River. The tracers in the branch streams are hard to flush out and the local residence time is much longer. The local residence time near the north bank of the reservoir is shorter than that near the south bank, probably due to the existence of Coriolis force and asymmetry of bottom topography. The regions where WAD happened usually have a short local residence time, and a front would establish between them and their adjacent wet areas where a long local residence time usually was determined.

3) Flows (including inflows and withdrawals) are the decisive influencing factors of the flushing characteristics of a reservoir. The stronger the inflows and withdrawals, the faster the tracers were flushed out. Heat fluxes are the controlling factors of the water flushing of a strong stratified reservoir, such as Dahuofang Reservoir. On one hand, heat fluxes induced density driven circulation can even the local residence time in the main reservoir and the branch streams. On the other hand, heat fluxes caused thermal stratification restricts mixing in the vertical direction and enhances the vertical difference of local residence time. Wind has the weakest effect on the water flushing of Dahuofang Reservoir. Even so, it should still be considered in the estimation of residence time of a reservoir, because that wind can strengthen the horizontal advection and vertical mixing, and therefore, even the local residence time distribution.

Finally, it should be noted that the conclusions obtained in this study are based on the hydrological and meteorological conditions of Dahuofang Reservoir in 2008, and the methodology used in this study is based on general water circulation (with a conservative tracer used as the indicator) rather than pollutant specific. Appropriate corrections should be considered depending on the pollutant analyzed.

Acknowledgements This research is supported by the National Natural Science Foundation of China (Grant No. 51279023) and by the National Basic Research Program of China (Grant No. 2013CB430403).

References

Ahsan A K M Q, Blumberg A F (1999). Three-dimensional hydrothermal model of Onondaga Lake, New York. J Hydraul Eng, 125(9): 912–923

Blanton J O, Garrett A J, Bollinger J S, Hayes D W, Koffman L D, Amft

J, Moore T (2010). Transport and retention of a conservative tracer in an isolated creek-marsh system. Estuar Coast Shelf Sci, 87(2): 333–345

Blumberg A F, Mellor G L (1987). A description of a three-dimensional coastal ocean circulation model. In: Heaps N S, ed. Three-Dimensional Coastal Ocean Models. Washington, DC: American Geophysical Union, 1–16

Boehrer B, Schultze M (2008). Stratification of lakes. Rev Geophys, 46 (2): RG2005

Bolin B, Rodhe H (1973). A note on the concepts of age distribution and transit time in natural reservoirs. Tellus, 25(1): 58–62

Camacho R A, Martin J L (2013). Hydrodynamic modeling of first-order transport timescales in the St. Louis Bay Estuary, Mississippi. J Environ Eng, 139(3): 317–331

Cavalcante G H, Kjerfve B, Feary D A (2012). Examination of residence time and its relevance to water quality within a coastal mega-structure: The Palm Jumeirah Lagoon. J Hydrol (Amst), 468–469: 111–119

Dabrowski T, Berry A (2009). Use of numerical models for determination of best sampling locations for monitoring of large lakes. Sci Total Environ, 407(14): 4207–4219

Dabrowski T, Hartnett M (2008). Modelling travel and residence times in the eastern Irish Sea. Mar Pollut Bull, 57(1–5): 41–46

Dabrowski T, Hartnett M, Olbert A I (2012). Determination of flushing characteristics of the Irish Sea: a spatial approach. Comput Geosci, 45: 250–260

de Brauwere A, de Brye B, Blaise S, Deleersnijder E (2011). Residence time, exposure time and connectivity in the Scheldt Estuary. J Mar Syst, 84(3–4): 85–95

Delhez É M, Deleersnijder É (2012). Residence and exposure times: when diffusion does not matter. Ocean Dyn, 62(10–12): 1399–1407

Dionne D, Therien N (1997). Minimizing environmental impacts of hydroelectric reservoirs through operational control: a generic approach to reservoirs in northern Quebec. Ecol Modell, 105(1): 41–63

Galperin B, Kantha L H, Hassid S, Rosati A (1988). A quasi-equilibrium turbulent energy model for geophysical flows. J Atmos Sci, 45(1): 55–62

Hellweger F L, Masopust P (2008). Investigating the fate and transport of Escherichia coli in the Charles River, Boston, using high-resolution observation and modeling. J Am Water Resour Assoc, 44 (2): 509–522

Hocking G C, Patterson J C (1994). Modelling tracer dispersal and residence time in a reservoir. Ecol Modell, 74(1–2): 63–75

HydroQual Inc (2002). A Primer for ECOMSED Version 1.3

Imberger J, Patterson J C (1989). Physical Limnology. Adv Appl Mech, 27: 303–475

Large W G, Pond S (1982). Sensible and latent heat flux measurements over the ocean. J Phys Oceanogr, 12(5): 464–482

Liu W, Chen W, Chiu C (2012). Numerical modeling of hydrodynamic and hydrothermal characteristics in subtropical alpine lake. Appl Math Model, 36(5): 2094–2109

Liu W C, Chen W B (2013). Modeling hydrothermal, suspended solids transport and residence time in a deep reservoir. Int J Environ Sci Technol, 10(2): 251–260

Ma F, Jiang C, Rauen W B, Lin B (2009). Modelling sediment transport processes in macro-tidal estuary. Science in China Series E: Technological Sciences, 52(11): 3368–3375

Madala R V, Piacseki S A (1977). A semi-implicit numerical model for baroclinic oceans. J Comput Phys, 23(2): 167–178

Mellor G L (2001). One-dimensional, ocean surface layer modeling: a problem and a solution. J Phys Oceanogr, 31(3): 790–809

Mellor G L, Yamada T (1982). Development of a turbulence closure model for geophysical fluid problems. Rev Geophys, 20(4): 851–875

Monsen N E, Cloern J E, Lucas L V, Monismith S G (2002). The use of flushing time, residence time, and age as transport time scales. Limnol Oceanogr, 47(5): 1545–1553

Oey L (2005). A wetting and drying scheme for POM. Ocean Model, 9 (2): 133–150

Oey L (2006). An OGCM with movable land–sea boundaries. Ocean Model, 13(2): 176–195

Oey L, Ezer T, Hu C, Muller-Karger F E (2007). Baroclinic tidal flows and inundation processes in Cook Inlet, Alaska: numerical modeling and satellite observations. Ocean Dyn, 57(3): 205–221

Patgaonkar R S, Vethamony P, Lokesh K S, Babu M T (2012). Residence time of pollutants discharged in the Gulf of Kachchh, northwestern Arabian Sea. Mar Pollut Bull, 64(8): 1659–1666

Phelps J J C, Polton J A, Souza A J, Robinson L A (2013). Hydrodynamic timescales in a hyper-tidal region of freshwater influence. Cont Shelf Res, 63: 13–22

Robins P E, Elliott A J (2009). The internal tide of the Gareloch, a Scottish Fjord. Estuar Coast Shelf Sci, 81(1): 130–142

Rosati A, Miyakoda K (1988). A general circulation model for upper ocean simulation. J Phys Oceanogr, 18(11): 1601–1626

Rueda F, Moreno-Ostos E, Armengol J (2006). The residence time of river water in reservoirs. Ecol Modell, 191(2): 260–274

Shen Y M, Wang J H, Zheng B H, Zhen H, Feng Y, Wang Z X, Yang X (2011). Modeling study of residence time and water age in Dahuofang Reservoir in China. Science China Physics, Mechanics & Astronomy, 54(1): 127–142

Simons T J (1974). Verification of numerical-models of Lake Ontario: Part I. Circulation in spring and early summer. J Phys Oceanogr, 4(4): 507–523

Smagorinsky J (1963). General circulation experiments with the primitive equations I. The basic experiment. Mon Weather Rev, 91 (3): 99–164

Smolarkiewicz P K (1984). A fully multidimensional positive definite advection transport algorithm with small implicit diffusion. J Comput Phys, 54(2): 325–362

Takeoka H (1984). Fundamental concepts of exchange and transport time scales in a coastal sea. Cont Shelf Res, 3(3): 311–326

Vallino J J, Hopkinson J C S Jr (1998). Estimation of dispersion and characteristic mixing times in Plum Island Sound Estuary. Estuar Coast Shelf Sci, 46(3): 333–350

van de Kreeke J (1983). Residence time: application to Small Boat Basins. J Waterw Port Coast Ocean Eng, 109(4): 416–428

Wang C F, Hsu M H, Kuo A Y (2004). Residence time of the Danshuei River estuary, Taiwan. Estuar Coast Shelf Sci, 60(3): 381–393

Wang J H, Shen Y M, Zhen H, Feng Y, Wang Z X, Yang X (2011). Three-dimensional numerical modelling of water quality in Dahuofang Reservoir in China. Science China Physics, Mechanics & Astronomy, 54(7): 1328–1341

Warner J C, Rockwell Geyer W, Arango H G (2010). Using a composite grid approach in a complex coastal domain to estimate estuarine residence time. Comput Geosci, 36(7): 921–935

Zhang W G, Wilkin J L, Schofield O M E (2010). Simulation of water age and residence time in New York Bight. J Phys Oceanogr, 40(5): 965–982

Zhang Y H, Zhang M (2011). Numerical simulation of hydrodynamics and waste water diffusion of Yangtze River Estuary affected by Three Gorges Project in flood season. Chinese Journal of Hydrodynamics, 26(4): 470–478 (in Chinese)

Zimmerman J T F (1976). Mixing and flushing of tidal embayments in the western Dutch Wadden Sea part I: Distribution of salinity and calculation of mixing time scales. Neth J Sea Res, 10(2): 149–191

AUTHOR BIOGRAPHIES

Ming Zhang, Ph.D. candidate at the State Key Laboratory of Coastal & Offshore Engineering, Dalian University of Technology, was born in 1985. He obtained his B.S. in the School of Water Resources and Hydropower Engineering, Wuhan University in 2005. He has worked as a Master-Doctor combined program graduate student at Dalian University of Technology since 2005. His research interests are mainly on Environmental Hydraulics and Computational Hydraulics, specifically on modeling hydrodynamics and water quality of estuaries, coastal waters, and reservoirs. Email: nxycyzm@163.com

Yongming Shen, Professor at the Dalian University of Technology, obtained his Ph.D., M.S., and B.S. from Chengdu University of Science and Technology in 1991, 1988, and 1983, respectively. After he received his Ph.D., he worked as a postdoctoral fellow at the State Key Laboratory of Coastal & Offshore Engineering, Dalian University of Technology for two years, and then joined the Dalian University of Technology as an Associate Professor. Currently, he is a Professor at Dalian University of Technology. His primary research interests are focused on the areas of Environmental Hydraulics and Computational Hydraulics, with special emphasis on modeling of hydrodynamics, water quality and oil spills for rivers and coastal waters. Dr. Shen has published over 194 journal papers. Email: ymshen@dlut.edu.cn